AEROSOL PARTICLE SIZE RETRIEVALS FROM THE COMPACT RECONNAISSANCE IMAGING SPECTROMETER FOR MARS

S.D. Guzewich, *NASA Postdoctoral Fellow, NASA Goddard Space Flight Center, Greenbelt, MD, USA (scott.d.guzewich@nasa.gov)*, **M.D. Smith,** *NASA Goddard Space Flight Center, Greenbelt, MD, USA,* **M.J. Wolff,** *Space Science Institute, Boulder, CO, USA*

Introduction: The Compact Reconnaissance Imaging Spectrometer for Mars (CRISM) is a hyperspectral visible and near-infrared spectrometer onboard the Mars Reconnaissance Orbiter (MRO) designed to examine surface mineralogy [Murchie et al., 2007]. CRISM also has atmospheric science goals of examining atmospheric aerosols (e.g., Wolff et al., 2009) and gas species (e.g., Toigo et al., 2013). During the MRO extended mission, CRISM has made periodic limb-viewing geometry observations of the atmosphere [Smith et al., 2013]. These limb scans produce vertical profiles of dust and water ice aerosols with high vertical resolution. Smith et al. [2013] described the results of these scans using a retrieval algorithm with an effective radius of 1.5 μm for dust and 2 μm for water ice particles. In this work, we discuss initial CRISM limb-viewing observation retrievals of dust and water ice aerosols using multiple particle sizes.

Background: The recent identification of discrete or "detached" layers of dust [Heavens et al., 2011; Guzewich et al., 2013] and the complex layering of clouds [Heavens et al., 2010; Benson et al., 2011] has provided new impetus to the determination of Martian aerosol particle sizes as a possible means to explain the persistence of these layers. Kahre et al. [2008] illustrates the logarithmically decreasing fall velocities for smaller dust particle sizes. Hence, small dust particles, once transported to high altitudes, may reside there over long time periods and not require consistent resupply from the surface.

The canonically referenced size for dust particle sizes is 1.5 μm, with some variation around that value, and 2 μm is most typically used for water ice particles [Wolff and Clancy, 2003; Clancy et al., 2003; Smith et al., 2013]. However, some evidence exists for dust particle sizes that are both smaller (e.g., Rannou et al., 2006) and larger (e.g., Clancy et al., 2003). Clancy et al. [2003] identified two distinct cloud populations, one with smaller 1-2 μm particle sizes that they preferentially identified in southern latitudes and higher altitudes elsewhere, and a second population with sizes of 3-4 μm which they associated with the aphelion cloud belt.

Data and Methods: During a CRISM limb scan, the MRO spacecraft is tilted to allow CRISM to scan upward and downward across the limb from the surface to above 100 km altitude. Sufficient radiance is typically available to produce a vertical profile from the near-surface to 50-60 km altitude. The sampling method produces pixel resolution of approximately 800 m at the limb tangent point. As part of the retrieval, we further average the central 40 pixels "across track" (parallel to the limb) to increase signal-to-noise ratio and perform a running average of three pixels perpendicular to the limb resulting in a vertical resolution of roughly 2 km.

For limb-geometry observations, the retrieval algorithm must treat the spherical geometry of the observation. This is accomplished through a "pseudo-spherical" approximation that has been extensively validated against an exact Monte Carlo technique. This technique is orders of magnitude faster than the Monte Carlo technique, while still producing comparable results [Wolff et al., 2006; Smith et al., 2013]. The forward radiative transfer model accounts for multiple scattering using the discrete ordinates method.

To determine particle size, the retrieval algorithm is provided with extinction coefficients and single-scattering albedos for 3 distributions of dust particle size (effective radii, $r_{eff,}$ of 0.5 μm, 1.0 μm, and 1.5 μm) and 3 distributions of water ice particle size (effective radii, $r_{eff,}$ of 1.0 μm, 2.0 μm, and 3.0 μm). The effective radii were chosen to span a range of values reported in the literature. The effective variance, $v_{eff,}$ for the dust particle sizes is 0.3 and for water ice is 0.1.

12 wavelengths are used in the retrieval (Figure 1). These wavelengths were tested against other wavelength combinations and found to produce the clearest delineation between the 6 types of aerosols in the retrieval algorithm and produce the best fit to the data. Selected wavelengths are weighted toward the water ice absorption feature near 2800 nm.

The CRISM limb scans began in late MY29 and approximately 16000 atmospheric profiles are included in this study. Based on the cadence of the observations, most fall in one of two pole-to-pole tracks roughly falling over the Tharis province in the western hemisphere and over Hellas Basin/Syrtis Major in the eastern hemisphere (Figure 2).

Uncertainties in our results source from a number of factors including the pseudo-spherical approximation, choice of parameters (e.g., number of streams) in the algorithm and choice of particle size distributions and associated scattering properties. Following Smith et al. [2013], we find the error in a

particular mixing ratio value to vary between .05-.2, depending on altitude, with the lowest errors in the 20-30 km altitude range.

Results: *Aphelion Cloud Belt:* As identified by Clancy et al. [2003], we find the Aphelion Cloud Belt (ACB) to be composed of larger of water ice particles. The r_{eff} = 3-μm ice particle size distribution appears to dominate the ACB with a significant contribution from the r_{eff} = 2-μm distribution particles as well. The smallest size distribution of water ice particles, r_{eff} = 1 μm, compose the uppermost layers of the ACB, in altitudes with generally lower mixing ratios (Figure 3). Indeed, tropical clouds in all seasons are dominated by larger water ice particles, whereas smaller particles are typically relegated to the highest retrieved altitudes.

Polar Hood: Because CRISM observations require sunlight, data at high latitudes in local winter is comparatively limited to that in lower latitudes. However, where data is available, some trends are present. In southern hemisphere winter, the small r_{eff} = 1.0 μm ice particles clearly dominate the polar hood, particularly at altitudes above 20 km (not shown). There is some minor contribution from the r_{eff} = 2.0 μm ice particle size distribution at 10-30 km and the r_{eff} = 3.0 μm particle size distribution is present only in the near-surface layer of the atmosphere. A similar pattern is present in the northern hemisphere, but the r_{eff} = 1.0 μm ice particle size distribution contributes relatively little opacity to the vertical column. The retrieval algorithm also produces a conspicuous layer of the smallest dust size distribution (r_{eff} = 0.5 μm) within the northern polar hood at L_s = 340-360° north of 60°N at 20-40 km altitude. This is a region of the atmosphere that is very cold in this season and is expected to be relatively devoid of dust. As our retrieval algorithm does not explicitly retrieve CO_2 ice aerosols, it is possible that this "dust" may in fact by CO_2 ice particles.

Dust Layers: The discrete dust layer in the tropics termed the "high altitude tropical dust maximum" by Heavens et al. [2011] and "lower dust maximum" by Guzewich et al. [2013] shows up clearly in the CRISM retrievals and follows the seasonal cycle described by Guzewich et al. [2013]. The dust layer is absent in early northern spring and then is present for the remainder of the year. In northern spring and early summer, we find that dust in this layer is predominantly our largest size distribution (r_{eff} = 1.5 μm) with a noticeable lack of the smallest size distribution (r_{eff} = 0.5 μm) of dust in this region of the atmosphere (Figure 4). This suggests that at this time of the year, at least, this dust layer is not formed by differentiation of particle sizes through gravitational sedimentation, but rather that some mechanism directly resupplies dust to this layer on a regular basis. However, this dominance of r_{eff} = 1.5 μm dust is short-lived. During the remainder of northern summer (L_s = 120-180°), the vertical distribution is opposite of what would be expected from gravitational sedimentation in the tropics. The smallest dust size distribution (r_{eff} = 0.5 μm) is present in the low altitudes, with r_{eff} = 1.0 μm dust above from 20-30 km altitude and then a thin layer of the largest dust (r_{eff} = 1.5 μm) dust from 30-40 km (Figure 5). For the remainder of the year, this dust layer appears as a fairly even mix of r_{eff} = 1.0 μm and r_{eff} = 1.5 μm dust size distributions. This suggests a seasonal effect to the mechanism that supplies this dust layer and/or a changing dust source region at different times of the year.

By contrast, dust at high altitudes, near the "upper dust maximum" reported by Guzewich et al. [2013] is consistently small (r_{eff} = 0.5 μm and 1 μm), with less contribution from the larger (r_{eff} = 1.5 μm) dust particles. This suggests that the population of dust particle sizes that initially reaches these high (>45 km) altitudes is biased toward smaller particles or that gravitational sedimentation is removing the larger dust particle sizes quickly. The presence of large dust at high altitudes at some latitudes and seasons suggests the later possibility is more likely, in our view.

Northern Hemisphere Dust: Dust in the Northern Hemisphere is noticeably biased to smaller particle sizes throughout the year, with this bias most evident in the less dusty first half of the Martian year (L_s = 0-180°). This can be seen in both Figures 4 and 5. No clear preference is seen between the r_{eff} = 1.0 μm or 0.5 μm dust size distributions, with a fairly even mix present during most seasons over the northern low latitudes. Small dust particles (r_{eff} = 0.5 μm) are favored at higher altitudes.

References:

Clancy, R. T., M. J. Wolff, and P. R. Christensen (2003), Mars aerosol studies with the MGS-TES emission phase function observations: Optical depths, particle sizes, and ice cloud types versus latitude and solar longitude, *J. Geophys. Res.*, **108**, doi:10.1029/2003JE002058.

Guzewich, S. D., E. R. Talaat, A. D. Toigo, D. W. Waugh, and T. H. McConnochie (2013), High-altitude dust layers on Mars: Observations with the Thermal Emission Spectrometer, J. Geophys. Res. Planets, 118, 1177–1194, doi:10.1002/jgre.20076.

Heavens, N. G., M. I. Richardson, A. Kleinböhl, D. M. Kass, D. J. McCleese, W. Abdou, J. L. Benson, J. T. Schofield, J. H. Shirley, and P. M. Wolkenberg (2011), Vertical distribution of dust in the Martian atmosphere during northern spring and summer: Observations by the Mars Climate

Sounder and analysis of zonal average vertical dust profiles, *J. Geophys. Res.*, **116**, doi:10.1029/2010JE003691.

Kahre, M. A., J. L. Hollingsworth, R. M. Haberle, and J. R. Murphy (2008), Investigations of the variability of dust particle sizes in the Martian atmosphere using the NASA Ames general circulation model, *Icarus*, **195**, 576–597, doi:10.1016/j.icarus.2008.01.023.

Murchie, S., et al. (2007), Compact Reconnaissance Imaging Spectrometer for Mars (CRISM) on Mars Reconnaissance Orbiter (MRO), *J. Geophys. Res.*, **112**, E05S03, doi:10.1029/2006JE002682.

Rannou, P., S. Perrier, J.-L. Bertaux, F. Montmessin, O. Korablev, and A. Rébérac (2006), Dust and cloud detection at the Mars limb with UV scattered sunlight with SPICAM, *J. Geophys. Res.*, **111**, doi:10.1029/2006HE002693.

Smith, M. D., M. J. Wolff, R. T. Clancy, A. Kleinböhl, and S. L. Murchie (2013), Vertical distribution of dust and water ice aerosols from CRISM limb-geometry observations, *J. Geophys. Res.Planets*,118,321–334, doi:10.1002/jgre.20047.

Toigo, A. D., M. D. Smith, F. P. Seelos, and S. L. Murchie (2013), High spatial and temporal resolution sampling of Martian gas abundances from CRISM spectra, J. Geophys. Res. Planets, 118, 89–104, doi:10.1029/2012JE004147.

Wolff, M. J., and R. T. Clancy (2003), Constraints on the size of Martian aerosols from Thermal Emission Spectrometer observations, *J. Geophys. Res.*, **104**, doi:10.1029/2003JE002057.

Wolff, M. J., et al. (2006), Constraints on dust aerosols from the Mars Exploration Rovers using MGS overflights and Mini-TES, *J. Geophys. Res.*, **111**, doi:10.1029/2006JE002786.

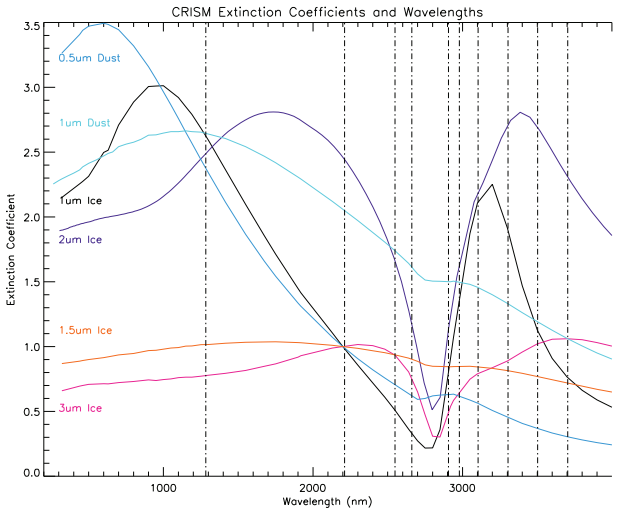

Figure 1. Extinction coefficients at wavelengths between 200 and 4000 nm for 3 dust and 3 water ice particle sizes (solid lines). Dash-dot lines indicate 12 wavelengths used in the retrieval algorithm.

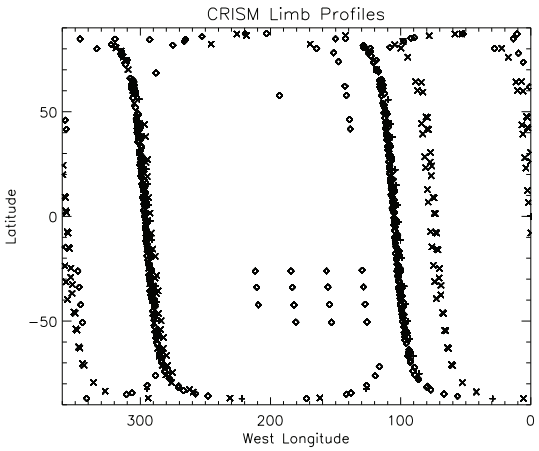

Figure 2. Locations of CRISM limb scans included in this study. Crosses denote MY29, diamonds MY30 and X's MY31.

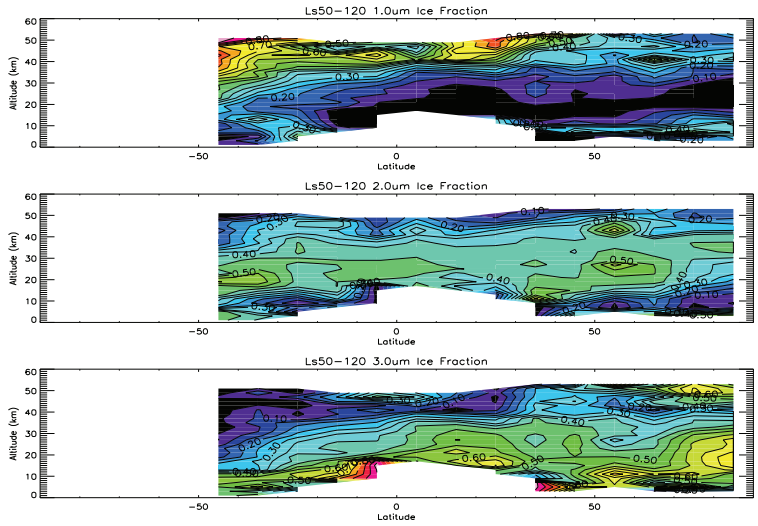

Figure 3. Fractional representation of each of the water ice particle size distributions for the Aphelion Cloud Belt season (L_s = 50-120°).

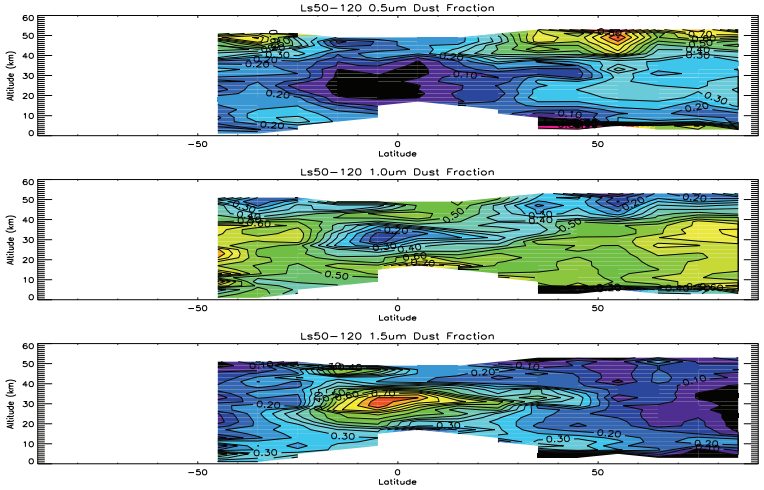

Figure 4. Fractional representation of each of the dust particle size distributions for L_s = 50-120°.

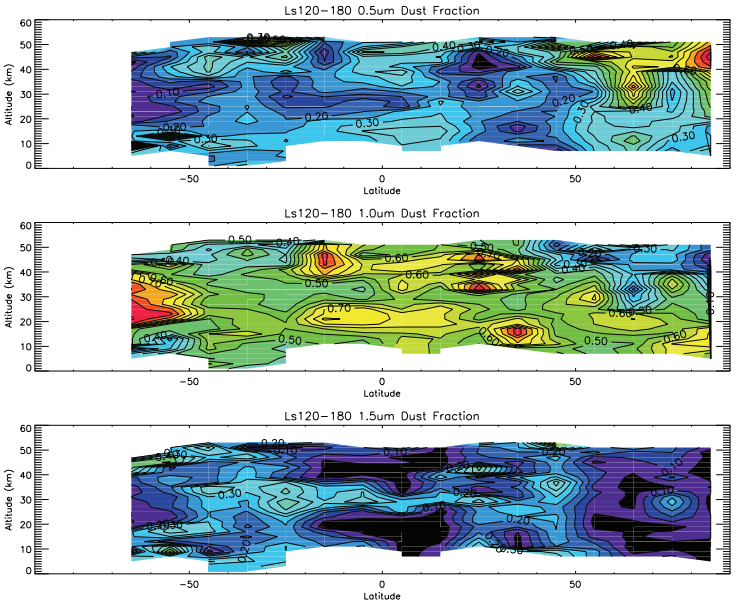

Figure 5. Fractional representation of each of the dust particle size distributions for L_s = 120-180°.